NeuroImage 329 (2026) 121803

Contents lists available at ScienceDirect

NeuroImage

journal homepage: www.elsevier.com/locate/ynimg

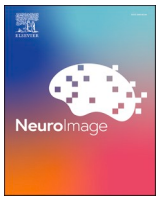

How vigilance states influence source imaging of physiological brain oscillations: Evidence from intracranial EEG

Xiaoyan Wei [a,b], Jawata Afnan [c,d,e], Tamir Avigdor [a,d,f], Nicolás von Ellenrieder [e], Édouard Delaire [k], Jessica Royer [g], Alyssa Ho [a], Erica Minato [e], Katharina Schiller [f], Kassem Jaber [a,b], Yingqi Laetitia Wang [f,l], Matt Moye [a], Boris C Bernhardt [g], Jean-Marc Lina [h,i,j], Christophe Grova [d,e,h,k,1], Birgit Frauscher [a,b,f,1,*]

[a] Analytical Neurophysiological Lab, Department of Neurology, Duke University, Durham, NC, USA
[b] Department of Biomedical Engineering, Duke University, Durham, NC, USA
[c] Integrated Program in Neuroscience, McGill University, Montréal, Québec, Canada
[d] Multimodal Functional Imaging Lab, Department of Biomedical Engineering, McGill University, Montréal, Québec, Canada
[e] Department of Neurology and Neurosurgery, Montreal Neurological Institute, McGill University, Montréal, Québec, Canada
[f] Analytical Neurophysiological Lab, Montreal Neurological Institute and Hospital, McGill University, Montreal, Quebec, Canada
[g] Multimodal Imaging and Connectome Analysis (MICA) Laboratory, McConnell Brain Imaging Centre, Montreal Neurological Institute and Hospital, McGill University, Montreal, Quebec, Canada
[h] Physnum Team, Centre De Recherches Mathématiques, Montréal, Québec, Canada
[i] Electrical Engineering Department, École De Technologie Supérieure, Montréal, Québec H3C 1K3, Canada
[j] Center for Advanced Research in Sleep Medicine, Sacré-Coeur Hospital, Montréal, Québec, Canada
[k] Multimodal Functional Imaging Lab, Department of Physics and Concordia School of Health, Concordia University, Montréal, Québec, Canada
[l] Schulich School of Medicine and Dentistry, Western University, London, ON, Canada

ARTICLE INFO

Keywords:
High-density EEG
Sleep/Wake physiology
Cortical oscillation analysis
Source imaging
Normative intracranial EEG
Vigilance states

ABSTRACT

Cortical oscillations across sleep-wake cycles are essential for coordinating functional brain dynamics. High-density electroencephalography (HDEEG) combined with electrical source imaging (ESI) provides a noninvasive approach to map cortical dynamics; however, its ability to capture spatial ongoing oscillations across different vigilance states remains uncertain. Here, we directly compared HDEEG source imaging by comparing it to a normative intracranial EEG (iEEG) atlas from 110 epilepsy patients with electrodes in healthy brain regions (https://mni-open-ieegatlas.research.mcgill.ca/). Wavelet-based Maximum Entropy on the Mean (wMEM) was applied to localize oscillatory patterns using overnight HDEEG recordings from 35 healthy adults (16 females, mean age 31.1 ± 6.3 years). Virtual iEEG (ViEEG) signals were estimated by applying an iEEG forward model to wMEM sources to examine oscillatory patterns across 5 frequency bands, 38 regions, and 4 vigilance states. We found that HDEEG source imaging exhibited comparable spectral patterns of iEEG in low frequencies but overestimated oscillatory activities at high frequencies. Lateral cortical regions exhibited more accurate source estimation than medial regions ($p < 0.05$). After removing the aperiodic components, the spectral alignment between ViEEG and iEEG significantly improved except for N3 sleep ($p < 0.05$). Oscillatory peak patterns in ViEEG reflect state-dependent dynamics that are broadly consistent with iEEG peaks ($p < 0.05$). HDEEG-derived ViEEG and magnetoencephalography-derived ViEEG approximated iEEG spectral features, showing complementary correspondence. These findings reveal that vigilance states significantly shape cortical oscillations by altering their spectral and spatial profiles. Our results establish HDEEG as a powerful tool for large-scale, noninvasive investigations of human sleep neurophysiology and brain network dynamics.

* Corresponding author at: Professor of Neurology and Biomedical Engineering, Analytical Neurophysiology Lab, Duke University, 2424 Erwin Road, Durham, NC 27705, USA.
E-mail address: birgit.frauscher@duke.edu (B. Frauscher).
[1] Shared senior authorship.

https://doi.org/10.1016/j.neuroimage.2026.121803
Received 25 October 2025; Received in revised form 30 January 2026; Accepted 11 February 2026
Available online 11 February 2026

1. Introduction

Cortical oscillations during the sleep-wake cycle reflect the brain's intrinsic state, supporting memory consolidation (Herweg et al., 2020), cognitive behavior (Ward, 2003), and large-scale neural communication (Buzsáki and Draguhn, 2004, Myrov et al., 2024). These rhythms are dynamic and state-dependent, varying in power, frequency, and spatial distribution across sleep stages. Despite their importance, the cortical oscillations in humans remain poorly understood. High-density electroencephalography (HDEEG) is an increasingly noninvasive technique for capturing neural activity with millisecond-level temporal resolution and full-head spatial coverage. These advantages enable detailed investigation of spontaneous brain activity across frequency bands in resting-state conditions (Lustenberger and Huber, 2012, Pigorini et al., 2023, Taberna et al., 2024, Zhou et al., 2023). However, compared to intracranial EEG (iEEG), the gold standard to measure neural activities, the spatial resolution of HDEEG remains limited due to the volume conduction effect (He et al., 2018) and low signal-to-noise ratio (SNR) (Pizzo et al., 2019).

To estimate the cortical sources, HDEEG must be paired with electrical source imaging (ESI), which aims to estimate the most likely source of the observed scalp EEG potentials by solving an ill-posed inverse problem that admits infinitely many solutions unless constrained by anatomical and biophysical priors (Michel and He, 2019). Moreover, ESI accuracy is known to be affected by signal spatial blurring, source leakage, and the difficulty of localizing deep or subcortical activity, especially during resting states that are characterized by low SNR in EEG signals (Kreidenhuber et al., 2019, Quintiliani et al., 2021). While prior studies have extensively applied noninvasive source imaging to characterize pathological activity, including epileptogenic zone localization (Abdallah et al., 2022, Sohrabpour et al., 2020), high-frequency oscillations (Cai et al., 2021), and interictal epileptiform discharges (Avigdor et al., 2024, Seeber et al., 2019, Cao et al., 2022), localizing spontaneous, ongoing cortical oscillations in the healthy brain remains a greater challenge due to low amplitude, lack of event markers, and variability across sleep stages.

Resting-state iEEG studies have revealed robust, state-specific spectral signatures in healthy cortical regions (Taylor et al., 2022), suggesting that vigilance states may systematically reshape oscillatory patterns. Yet, it remains unknown to what extent noninvasive ESI preserves this spatial and spectral specificity, especially during sleep. To address this question, we leveraged the MNI iEEG atlas, a publicly available dataset developed by our group that aggregates intracranial recordings from 110 patients with drug-resistant focal epilepsy (Frauscher et al., 2018, Von Ellenrieder et al., 2020). The atlas includes only electrodes located in healthy brain regions and provides dense spatial sampling across 38 cortical regions defined by the Medical Image Computing and Computer-Assisted Intervention (MICCAI) anatomical atlas (Landman and Warfield, 2012). It comprises over 2,300 channels during wakefulness, 2,149 channels during NREM (N2/N3), and 1,490 channels during REM stage, enabling normative characterization of cortical oscillations across vigilance states. It provides a rare opportunity to benchmark noninvasive source imaging against intracranial recordings across brain states.

In this study, we systematically examine properties of cortical oscillations from noninvasive HDEEG source imaging, comparing with ground-truth iEEG using a cross-modal framework. We hypothesize that the HDEEG source imaging could preserve the spatial and spectral oscillatory patterns aligned with those observed in iEEG, and shifts in vigilance states might influence HDEEG source imaging accuracy. We applied the wavelet-based Maximum Entropy on the Mean (wMEM) method to solve the inverse problem in the context of resting state HDEEG source imaging. wMEM is built upon the MEM source imaging framework, for which we carefully demonstrated excellent spatial properties in recovering the spatial extent of underlying generators of Magnetoencephalography (MEG) and HDEEG data when compared to commonly used linear source imaging methods for both MEG and HDEEG (Chowdhury et al., 2016, Hedrich et al., 2017, Pellegrino et al., 2020, Afnan et al., 2024). It's specifically tailored to localize oscillatory brain activity in EEG/MEG signals by leveraging a discrete wavelet transform (Daubechies wavelets), enabling frequency-resolved source estimation, which benefits from the MEM solver's excellent spatial properties (Lina et al., 2014). We previously showed that wMEM improves the localization of the spatial extent of underlying generators compared with minimum norm estimates (MNE) (Afnan et al., 2024) and improves the localization of resting-state oscillatory patterns compared with both MNE and beamformers (Afnan et al., 2023). We notably carefully adapted the wMEM method when applied to low SNR resting state data, through its initialization and baseline covariance estimation (using a sliding-window and phase-randomization strategy, see Appendix in (Afnan et al., 2023)). The wMEM approach has been successfully applied to recover the location and spatial extent of the underlying oscillatory generators of fast oscillations (Avigdor et al., 2021), ictal oscillations (Pellegrino et al., 2016), and oscillatory patterns during wakefulness (Afnan et al., 2023, Aydin et al., 2020). For those reasons, we believe the wMEM framework is appropriate to assess the accuracy of resting state HDEEG source imaging. To our knowledge, this is the first demonstration of a comprehensive study validating source imaging derived from HDEEG against the gold standard iEEG across vigilance states in healthy brain regions.

2. Materials and methods

2.1. Experimental design

Our analysis pipeline is presented in Fig. 1. For all participants, sections of 60-second ongoing wake and sleep HDEEG data were localized along the cortex using the wMEM framework (Afnan et al., 2024, Afnan et al., 2023, Lina et al., 2014), a distributed source localization method dedicated to the localization of oscillatory components. After co-registering the position of all the iEEG contacts of the MNI iEEG atlas within each subject-specific space, HDEEG source maps were projected into the iEEG space by estimated Virtual iEEG (ViEEG) signals, applying an iEEG forward model to HDEEG source maps (Abdallah et al., 2022, Afnan et al., 2023, Grova et al., 2016). Spectral power, oscillatory components, and spectral peaks were then computed for ViEEG and compared against iEEG ground-truth data across 38 cortical regions of interest (ROIs).

2.2. Study participants

45 healthy adults (range: 18–45 years) were recruited between March 2022 and December 2024. Participants were screened for eligibility based on the absence of neurological or psychiatric conditions, sleep disorders, and the use of medications known to affect sleep or cognitive functions, following previously published criteria (Wei et al., 2024). Participants were also required to score below 5 on the Pittsburgh Sleep Quality Index, indicating good sleep quality. Eligible individuals underwent overnight HDEEG and polysomnography recordings at the sleep lab of McGill University Health Centre Research Institute.

After preprocessing and sleep scoring of data, we further excluded 9 participants with an Apnea–Hypopnea Index (AHI) greater than 15 events per hour and 1 participant due to issues with digitized electrode positions. (Fig. 2A). The final dataset comprised 35 healthy adults (16 females, mean ± SD age, 31.1 ± 6.3 years). The average sleep time is approximately 333.6 ± 81.4 minutes, and sleep efficiency is 80.5 + 13.3% (Fig. 2B).

3. Ethics statements

All study participants signed written informed consent according to

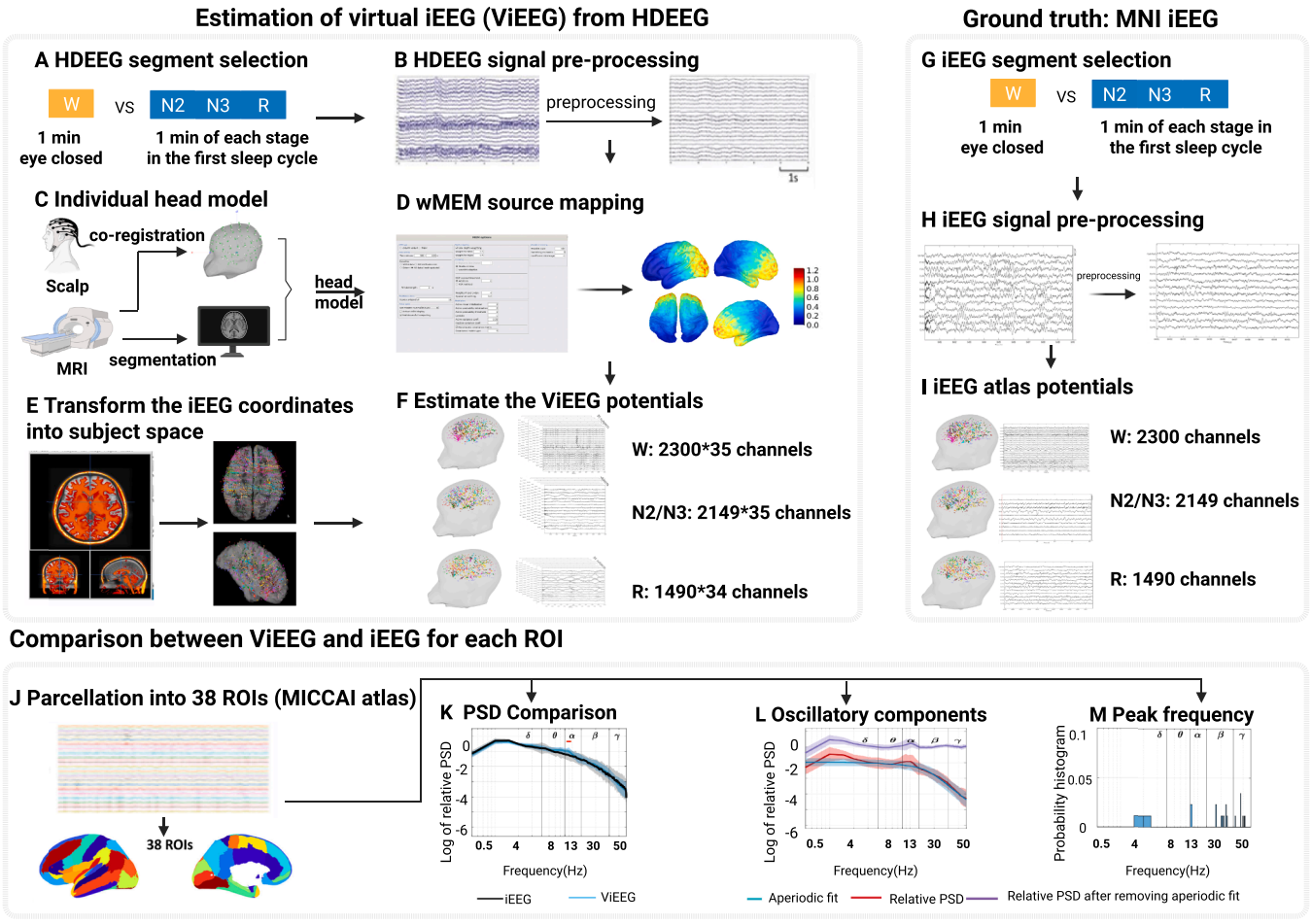

Fig. 1. Conceptual workflow of data analysis. **A** HDEEG sections of 60s from wake, N2, N3, and REM stages for each subject. **B** HDEEG signal pre-processing employing manual inspection, filtering, down-sampling, and artifact removal with Signal-Space Projection (SSP). **C** Individual MRI data and co-registered electrodes were combined to generate the head model. **D** wMEM source mapping using our plugin implemented in Brainstorm (https://neuroimage.usc.edu/brainstorm/Tutorials/TutBEst). **E** The positions of the iEEG channels were projected from the template ICBM152 anatomy to the anatomy of each healthy subject. **F** ViEEG potentials at each position of iEEG channels (positions obtained from the MNI iEEG atlas) were estimated from wMEM maps. **G** 60s iEEG segments were selected from the iEEG MNI atlas from the wake, N2, N3, and REM stages, respectively. **H** iEEG signal pre-processing using manual inspection, filtering, down-sampling, and artifact removal with SSP. **I** The clean iEEG data was used to compare with the ViEEG after pre-processing. **J** Parcellation of the iEEG into 38 ROIs: The channels in the atlas were classified into 38 ROIs based on the MICCAI atlas (Landman and Warfield, 2012). **K** Computation of the power spectral density (PSD). **L** Oscillatory components analysis by removing the aperiodic components using the Fitting Oscillations & One Over F (FOOOF) toolbox (Tiwari et al., 2023). **M** The distribution of oscillatory peaks in both ViEEG and iEEG data was analyzed in each region using the FOOOF toolbox. Abbreviations: PSD, power spectral density; ViEEG, virtual intracranial EEG; iEEG, intracranial EEG; ROIs, Regions of interest ; Fitting Oscillations & One Over F, FOOOF.

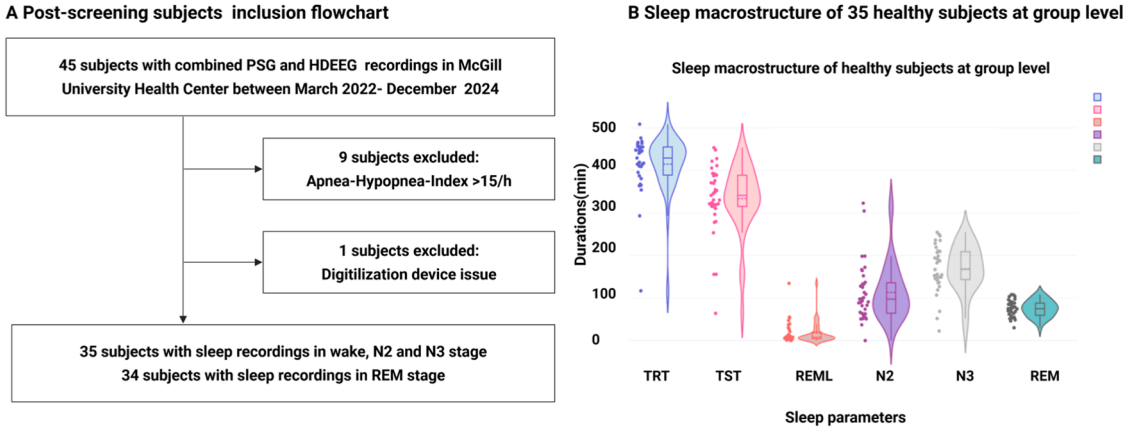

Fig. 2. Selection criteria of healthy subjects and general sleep characteristics. **A** Post-screening subject inclusion flowchart. **B** Sleep macrostructure box plot of 35 subjects at the group level, including total record time (TRT), total sleep time (TST), REM latency (REML), N2, N3, and REM duration.

the study protocol approved by the Research Ethics Board of the Montreal Neurological Hospital and Institute (MP-37-2018-3886), and all procedures were performed by the 1964 Helsinki Declaration and its later amendments.

3.1. Ground truth: iEEG atlas

The MNI iEEG Sleep Atlas (Frauscher et al., 2018, Von Ellenrieder et al., 2020) describes brain activity across vigilance states and cortical regions. It includes Wake, N2, N3, and REM stage recordings, collected ≥72 hours post-stereo-EEG implantation or ≥1 week after subdural grid/strip placement, with a minimum sampling rate of 200 Hz. Data were acquired ≥12 hours post-generalized seizure and ≥6 hours post-focal seizure, with wake-stage recordings taken with eyes closed. Electrodes were localized peri-implantation, projected onto the ICBM152 template, and only non-epileptic, non-lesional channels were included (Wake: 2300; N2/N3: 2149; REM: 1490), each with 60 seconds of resting-state data. Channels were classified into 38 ROIs using the MICCAI atlas (Landman and Warfield, 2012), combining both hemispheres. The dataset includes recordings from 110 patients (age: 31 ± 10 years, range: 13-62 years), with a total of 2,300 channels during wakefulness, 2,149 channels during NREM, and 1,490 channels during REM, projected onto 38 cortical regions based on the MICCAI atlas. Further methodological and anatomical details are described (Frauscher et al., 2018, Von Ellenrieder et al., 2020).

3.2. HDEEG data selection

Overnight polysomnography and HDEEG recordings were acquired using a JE-120 amplifier system (Nihon Kohden, Tokyo, Japan). Electrode placement followed the international 10–10 system (Avigdor et al., 2021). Of these, 83 electrodes were glued to the scalp using collodion, with impedances maintained below 5 kΩ. Data were sampled at 1000 Hz.

To ensure direct comparability with the ground-truth iEEG atlases, we matched the same segment duration and selection strategy outlined in the MNI iEEG wake (Frauscher et al., 2018) and sleep atlases (Von Ellenrieder et al., 2020), where one artifact-free 60-second segment was selected for each subject per vigilance state. Previous work (Wiesman et al., 2022) has shown that the duration of short segments(30-120 seconds) allows robust estimation of both rhythmic and arrhythmic spectral components of intrinsic brain activity, regardless of instrument technology and resting-state paradigm. Furthermore, 60-second resting-state segments in intracranial EEG and scalp research are sufficient to provide reliable estimates of power spectral density and oscillatory activity (Frauscher et al., 2018, Von Ellenrieder et al., 2020, Afnan et al., 2023). Accordingly, approximately 60 s of resting-state data were analyzed per sleep stage in the present study.

Regarding segment selection, resting-state HDEEG data were visually identified as either continuous recordings or concatenated artifact-free segments, with each segment lasting at least 5 seconds. This minimum duration was chosen to balance temporal continuity with sufficient total data length, consistent with prior work (Frauscher et al., 2018, Von Ellenrieder et al., 2020). For wakefulness, a single 60-second eyes-closed resting-state segment was selected per subject, since eyes-closed awake segments were selected in the MNI iEEG atlas. For sleep, 60-second HDEEG segments from stages N2, N3, and REM during the first sleep cycle were analyzed. The first sleep cycle was selected to minimize the confounding effects of sleep homeostasis and state-dependent changes in sleep microstructure. If 10 minutes of sleep data were not available within the first cycle, segments from the second cycle were used to complete the dataset. This follows the methodology of MNI iEEG atlases (Frauscher et al., 2018, Von Ellenrieder et al., 2020), with the same segment selection criteria applied to both HDEEG and iEEG recordings to ensure comparable experimental conditions across modalities. All segments were visually inspected and confirmed to be free of artifacts by a board-certified polysomnography technologist.

3.3. EEG signals preprocessing

Signal preprocessing was performed using the Brainstorm (Tadel et al., 2011) software package, implemented in MATLAB (MathWorks, Natick, MA). It included the following steps: 1) Bandpass filtering the data between 0.5 to 50 Hz and down-sampling to 200 Hz. 2) Applying a notch filter at 50 & 60 Hz in iEEG data. 3) Removal of cardiac and eye movement artifacts using SSP routine (Uusitalo and Ilmoniemi, 1997). 4) Visual inspection of HDEEG epochs to ensure the signal quality.

3.4. Head modeling

Each subject underwent a T1-weighted (T1w) structural scan at the Brain Imaging Centre of the Montreal Neurological Institute and Hospital, using a 3T Siemens Magnetom Prisma-Fit scanner equipped with a 64-channel head coil. Subsequent brain segmentation and reconstruction of the white/gray matter interface were performed using micapipe (Cruces et al., 2022), an open-access processing pipeline that utilizes FreeSurfer for anatomical reconstruction(https://micapipe.readthedocs.io/).

The HDEEG electrode locations for each subject were digitized using 3D FastTrack by Polhemus and co-registered with their individual anatomical MRI in Brainstorm by aligning the MRI-derived head surface with the digitized head shape and fiducial landmarks recorded during HDEEG acquisition. The cortical mesh used as the source space was extracted from the mid-layer between white and gray matter boundaries and then downsampled to result in approximately 9,000 vertices, covering both lateral and mesial cortical surfaces. We also added the hippocampus as a surface mesh in our source model (Afnan et al., 2024). The individual head model was generated using a 3-layer Boundary Element Model implemented in the OpenMEEG software (Gramfort et al., 2010), consisting of the brain, skull, and scalp surfaces, with conductivity values of 0.33, 0.0165, and 0.33 S m^{-1}, respectively (Acar et al., 2016).

3.5. HDEEG Source imaging using wMEM

The inverse problem of EEG source imaging was solved within the Maximum Entropy on the Mean framework (Chowdhury et al., 2016, Amblard et al., 2004). MEM is a distributed source localization technique that leverages a Bayesian spatial prior model assuming brain activity to be organized within cortical parcels. The activity of every parcel is scaled by the probability of activation of every parcel, which is tuned through a hidden state variable. When the parcel is active, a Gaussian distribution is used as the prior of the activity within the parcel. When the parcel is inactive, a Dirac distribution is considered that allows shutting down the activity from this parcel. Starting from such a prior "reference" prior distribution, the model is fitted to data by maximizing the relative entropy between the solution and the prior. As a result, MEM can either switch off or switch on the parcels during the localization process, while still allowing local contrast on the cortical surface within the active parcels. Parcellation of the whole cortical surface and initialization of the probability of being active were obtained using a data-driven approach, based on a Multivariate Source Pre-localization (MSP) method (Mattout et al., 2005), a projection technique allowing to define the probability of every source to contribute to the data. MEM provides accurate localization of the generators together with their spatial extent, as demonstrated by the standard variants of MEM, coherent MEM (cMEM) (Abdallah et al., 2022, Chowdhury et al., 2016, Chowdhury et al., 2013) and wavelet-based MEM (wMEM) (Afnan et al., 2023, Lina et al., 2014, Afnan et al., 2025). wMEM applies a discrete wavelet transformation (Daubechies wavelets) of the data before applying the MEM solver. We demonstrated its distinctive capability to identify the oscillatory patterns at seizure onset (Pellegrino et al., 2016),

interictal fast oscillations (Avigdor et al., 2021, von Ellenrieder et al., 2016), resting state connectivity patterns (Aydin et al., 2020), and validated its ability to capture resting state oscillations and connectivity with iEEG (Afnan et al., 2023, Afnan et al., 2025). The wMEM method is available within the Brain Entropy in space and time (Best) plugin of Brainstorm software (https://neuroimage.usc.edu/brainstorm/Tutorials/TutBEst).

We used the latest wMEM version, which was adapted for localizing low-SNR resting-state activity (Afnan et al., 2023), and for localizing deep brain activity by incorporating a depth-weighting parameter proposed and validated in MEG studies (Afnan et al., 2024). This version was further validated for reconstructing MEG resting-state oscillations and connectivity during the wake state using the MNI iEEG atlas (Afnan et al., 2023, Afnan et al., 2025). The depth weighting parameter was set to 0.5. In terms of baseline estimation for resting-state data, a quasi-synthetic baseline was generated by randomly altering the Fourier phase at each frequency (Prichard and Theiler, 1994). We employed a sliding window approach (window length: 1 s) to generate the baseline, ensuring a more precise estimation of the noise covariance matrix for each wavelet sample across the scales (Afnan et al., 2023).

3.6. Estimation of virtual iEEG from HDEEG source map

To enable a quantitative comparison between HDEEG signals and iEEG recordings, we transformed HDEEG source maps into ViEEG signals. To achieve this transformation, firstly, the positions of the iEEG atlas-defined electrode contacts need to be co-registered within each subject's native MRI coordinate system. Since the iEEG electrodes were originally projected onto the standardized ICBM152 template, each subject's MRI was co-registered with this standard using a three-step process developed by the minctracc program (Collins et al., 1994) : (1) estimation of a linear registration to account for the linear part of the transformation (using bestlinreg_s tool), (2) estimation of a non-linear transformation to account for the variability between the two maps (using minctracc tool); (3) application of the resulting non-linear transformation to the coordinates of the electrode contacts of MNI iEEG atlas, to convert them from the ICBM152 anatomy to the anatomy of each healthy subject.

We then estimated the virtual iEEG potentials from the HDEEG source map for each subject following the method proposed by Grova et al (Grova et al., 2016). To do so, we considered HDEEG-reconstructed source map J_{HDEEG} and subject-specific iEEG forward model G_{iEEG}, which quantifies the contribution of each dipolar source to the cortical surface for each iEEG channel (Grova et al., 2016). Since we did not intend to solve the inverse problem of source localization from iEEG data, we considered a simplified iEEG forward model G_{iEEG}, assuming an infinite volume conductor with a conductivity (σ) of 0.25 $S.m^{-1}$. To avoid numerical instabilities, when the sources on the cortical surface were too close to the iEEG contacts (distance < 3 mm), the distance was set to 3 mm instead in these estimations G_{iEEG}, while keeping the original orientations between the dipolar source orthogonal to the cortical surface and the electrode location, see (Grova et al., 2016) for further details.

With a total number of iEEG contacts c (c was 2300 for stage W, 2149 for stage NREM, and 1490 for stage REM) and number of cortical sources (n = 9000), G_{iEEG} is a $c \times n$ matrix that estimates the electrical potential at each iEEG electrode ($i = 1, 2, \ldots c$), corresponding to an equivalent current dipole of unit activity located at vertex $S_j$and oriented along j, normal to the cortical surface ($j = 1, 2, \ldots n$), calculated as:

$$V_{iEEG} = G_{iEEG} J_{HDEEG} \quad (1)$$

For each source map obtained from all 35 participants, we estimated the virtual iEEG (ViEEG) for each iEEG channel across all vigilance states. This resulted in more channels in ViEEG compared with the iEEG atlas. Specifically, it generated data from 2,300 channels in the iEEG atlas versus 2,300 × 35 channels in the ViEEG in the wake stage, 2149 channels in the iEEG atlas versus 2149 × 35 channels in the ViEEG in the NREM stage, while 1490 channels in the iEEG atlas versus 1490 × 34 channels in the ViEEG in the REM stage, as one subject was excluded from the REMstage analysis due to insufficient artifact-free REM data.

3.7. Analyses of relative power for specific frequency maps

For each iEEG and ViEEG channel, the power spectral density (PSD) was estimated using Welch's method (Time duration: 0-60 s, 2-s sliding Hamming windows, overlap: 50%). A relative PSD for each channel was obtained by dividing each PSD value by the total power across the entire frequency range. The group average of the relative PSD was calculated across all channels within a ROI and all frequency bins in each frequency band of interest: delta (0.5-4 Hz), theta (4-8 Hz), alpha (8-13 Hz), beta (13-30 Hz), and low gamma (30-50 Hz). The frequency range (0.5–50 Hz) was divided into 100 bins with 0.5-Hz resolution. To compare the relative PSD before and after converting the HDEEG source maps into virtual intracranial space, we also calculated the relative PSD after HDEEG source imaging directly along the cortical surface in the Supplementary Figure 1 by computing a group average of the relative PSD from healthy subjects after realigning the cortical surfaces of every subject to a surface template space.

3.8. Analyses of spectral oscillatory components and peak frequency

The (FOOOF) algorithm (Donoghue et al., 2020) was used to separate the periodic and aperiodic components of the power spectra by modeling the PSD as a combination of both. The algorithm employs an iterative fit-refit process, where the aperiodic component is represented by an exponential function, and each periodic component is modeled using a Gaussian function. For each iEEG and ViEEG channel, we applied the FOOOF algorithm to decompose the power spectra into periodic and aperiodic components. The following FOOOF parameters were used: frequency range = 0.5–50 Hz; peak type = Gaussian; peak width limits (minimum bandwidth, maximum bandwidth) = 1–8 Hz; maximum number of peaks = 8; peak threshold = 3.0 dB; proximity threshold = 2 SD; aperiodic mode = knee. Since our focus was on rhythmic activities in the spectra, we subtracted the aperiodic component (in the log-log scale) from the raw PSD. The remaining oscillatory component of the spectra (PSD iEEG and PSD ViEEG) was then used for further analysis and comparison between iEEG and ViEEG. Additionally, we identified the specific oscillatory peaks during the fitting process of extracting the aperiodic components.

3.9. Quantitative comparison of ViEEG and iEEG regarding power spectra and peak frequency

For spectral comparison, we computed an *overlap* metric to quantify the distance between the ViEEG and iEEG power spectra. To do so, first, we computed the median PSD for both iEEG and ViEEG. Specifically, the median of PSD_{iEEG} ($MPSD_{iEEG}$)was calculated based on the available channels from all participants within the ROI in the iEEG atlas. Similarly, for ViEEG, the median of PSD_{ViEEG} ($MPSD_{ViEEG}$) for each ROI was obtained across the total number of channels (number of channels within ROI in each subject's ViEEG x number of healthy subjects). Then, we calculated the standard deviation of PSD_{ViEEG} name as SD_{ViEEG}. The overlap between PSD_{iEEG} and PSD_{ViEEG} was calculated for each frequency bin using Equation (2).

$$\text{overlap} = \begin{cases} 1 - \dfrac{|MPSD_{iEEG} - MPSD_{ViEEG}|}{SD_{ViEEG}}, & if \quad |MPSD_{ViEEG} - MPSD_{iEEG}| \leq SD_{ViEEG} \\ 0, & otherwise \end{cases} \tag{2}$$

The overlap value for each frequency bin ranges between 0 and 1 (calculated for 100 frequency bins). We calculated the overlap for each ROI before and after removing the aperiodic components of the spectra, then obtained the average overlap across all the frequency bins within each frequency band of interest.

In terms of the peak frequency comparison, we calculated the Peak estimation metric as a percentage that quantifies the overestimation or underestimation of HDEEG-estimated ViEEG channels showing oscillatory peaks when compared to ground-truth iEEG peaks (Afnan et al., 2023). For each ROI in individual subjects, we determined the number of channels (out of the total number of channels in that ROI, N_{ROI}) that exhibited an oscillatory peak within a specified frequency band for both iEEG and ViEEG. Then we computed Peak_Estimation as the percentage difference in the number of channels showing peaks in ViEEG relative to iEEG, normalized by the total number of channels in each ROI and frequency band as described in Equation (3)

$$\text{Peak\_Estimation} = \frac{N_{peak\_ViEEG} - N_{peak\_iEEG}}{N_{ROI}} * 100\% \tag{3}$$

Where N_{peak_ViEEG} represents the number of channels exhibiting peaks in ViEEG for a given frequency band, while N_{peak_iEEG} denotes the number of channels exhibiting peaks in iEEG for a given frequency band. We calculated the median of Peak_Estimation over 35 subjects to obtain the group-level estimation of channels exhibiting peaks per ROI per frequency band. From the equation, the Peak_Estimation ranges from -100% to +100%. The +100% presents the 100% overestimation of ViEEG compared with iEEG; it indicates that all the ViEEG channels in that ROI (NROI) showed peaks in that frequency band, whereas no peak was identified in any of the iEEG channels in that ROI and frequency band. The -100% represents the complete opposite.

3.10. Statistics analysis

To assess differences in relative PSD between iEEG and ViEEG, the normality of the relative PSD distributions was assessed using the Shapiro–Wilk test. As many regions violated the assumption of normality ($p < 0.05$), the Welch's unequal variances t-test was employed. A significance threshold of $p < 0.05$ was applied, with Bonferroni correction implemented to control multiple comparisons across 38 regions of interest (ROIs) and 5 distinct frequency bands. For the comparison of iEEG

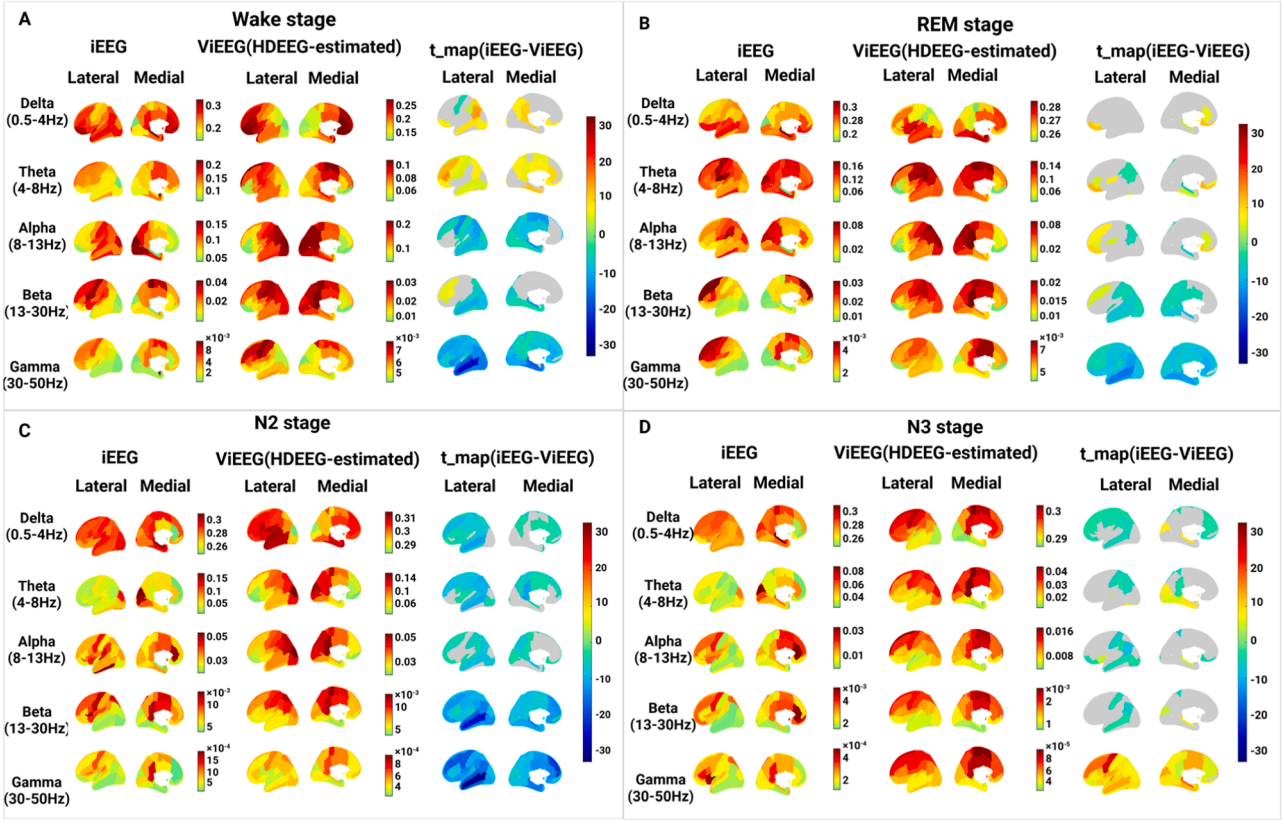

Fig. 3. Group-averaged relative PSD across five frequency bands and 38 ROIs for both iEEG (left) and ViEEG (middle) in each subplot: A (Stage W), B (Stage R), C (Stage N2), and D (Stage N3). Relative PSD for each channel was computed as the power ratio in each frequency band to the total signal power, yielding values between 0 and 1. The color bar of relative PSD ranges from the minimum to the maximum value and is specific to each modality. The right panel of each subplot highlights ROIs exhibiting significant differences in PSD between iEEG and ViEEG (Welch's t-test, $p < 0.05$, multiple comparisons Bonferroni correction applied across 38 ROIs and 100 frequency bins); the t-maps share a common color scale. Negative t-values indicate regions where iEEG power was significantly lower than ViEEG, reflecting an overestimation of spectral power by ViEEG. Abbreviations: PSD, power spectral density; ViEEG, virtual intracranial EEG; iEEG, intracranial EEG; ROIs, Regions of interest.

and ViEEG spectra after the removal of aperiodic components, statistical differences were evaluated using the non-parametric Mann-Whitney U test. A significance threshold of $p < 0.05$ was applied, with Bonferroni correction accounting for multiple comparisons across 38 ROIs and all frequency bins. For all Mann–Whitney U tests, effect sizes were quantified using Cliff's delta (δ), which is appropriate for non-parametric two-sample comparisons and facilitates interpretation of the magnitude of observed effects. The reported effect size (δ) corresponds to the median Cliff's d across all comparisons as the data distribution is not normal.

4. Results

4.1. ViEEG reliably reconstructs comparable low-frequency spectral patterns across vigilance states but discrepancies in gamma activities

We examined the power spectral distribution of 38 cortical regions across canonical frequency bands, both iEEG and HDEEG-derived ViEEG across four vigilance states: wakefulness, REM, N2, and N3 sleep (Fig. 3). Supplementary Figure 1 presented a comparison between relative power estimates obtained along the cortical surface from HDEEG source maps and estimation within the MNI iEEG space computed from ViEEG data, demonstrating that ViEEG preserved the overall spectral distribution of the cortical source estimates.

Overall, we observed ViEEG recovered the canonical low-frequency spectral power across states, while gamma showed frequency- and state-specific biases. During wakefulness, both iEEG and ViEEG showed dominant alpha power in the posterior regions (Fig. 3A, Supplementary Figure 2A) and beta power in frontal regions. t-maps revealed regional positive t-values in low-frequency bands (delta, theta, and beta), indicating significantly higher power in iEEG in a few regions ($p < 0.05$). Gamma power, by contrast, was overestimated by ViEEG in lateral and posterior areas. During stage R (Fig. 3B, Supplementary Figure 2B), alpha activity from ViEEG resembled iEEG more, and the low-frequency (delta, theta, and alpha) mismatched between ViEEG and iEEG diminished, as reflected by smaller regional t-values. Gamma-band overestimation remained prominent in posterior regions, while beta discrepancies were modest. In NREM sleep, especially N2 and N3, ViEEG closely matched iEEG in delta and theta bands, particularly during N3, where low-frequency agreement was strongest (Fig. 3C–3D, Supplementary Figure 2C-2D). Beta power showed overestimation in posterior areas across both NREM stages. Gamma-band discrepancies exhibited state-dependent variability across NREM stages, with overestimation by ViEEG prominent during N2 but reversed during N3 sleep.

4.2. Removal of the aperiodic component improves the ViEEG-iEEG spectral alignment except for N3 sleep

After characterizing ViEEG power distributions across vigilance states, we quantified the spectral overlap value across all 38 ROIs both before and after aperiodic component removal in Fig. 4, and found that removing the aperiodic (1/f-like) background improved spectral agreement between ViEEG and iEEG. Also, to illustrate region-specific effects, we chose two representative regions (angular gyrus from the lateral area, anterior cingulate from medial areas) to show statistically significant differences in each frequency band (Mann-Whitney U test, Bonferroni corrected $p < 0.5$). Power spectral comparisons before (blue line) and after aperiodic removal (orange line) across all 38 ROIs and vigilance states are shown in Supplementary Figure 3–Figure 6.

During wakefulness, removing aperiodic components markedly increased spectral overlap across most cortical regions (Fig. 4A). In the angular gyrus (superficial region, Fig. 4B), for example, the overlap improved in delta (0.07/0.48), theta (0.19 /0.50), and beta (0.66 /0.75) bands during wakefulness. In stage R, a similar improvement was observed primarily in low-frequency bands (Fig. 4C). The overlap increased in delta (0.59/0.66), theta (0.45/0.81), and alpha (0.3 /0.72), while the beta (0.67/0.62) and gamma (0.28/ 0.17) overlap decreased, indicating a frequency-dependent effect in the angular gyrus (Fig. 4D). During N2 sleep, the aperiodic removal improved overlap across most bands (Fig. 4E). In the angular gyrus, overlap rose in delta (0.06/ 0.22), theta (0.11/0.41), alpha (0.12/0.41), and beta (0.36/0.69) (Fig. 4F). In contrast, during N3, the overlap between ViEEG and iEEG in the angular gyrus remained consistently low and even declined slightly following the removal of the aperiodic component (Fig. 4G–4H). Similar patterns were also observed in the anterior cingulate regions.

4.3. ViEEG estimates are more accurate in lateral than medial regions

After removing the aperiodic component, we computed spectral-overlap maps for 38 cortical regions covering lateral and medial surfaces (Fig. 5; Supplementary Figures 3–Figure 6). Across vigilance states, lateral cortical regions showed consistently higher ViEEG–iEEG alignment than medial structures (Mann–Whitney U test, Bonferroni-corrected $p < 0.05$, median $\delta = 0.39$). Representative spectra from the middle temporal gyrus (lateral) and the hippocampus (medial) illustrate this pattern (Fig. 5A–5B). In the middle temporal gyrus, ViEEG estimates (orange) closely matched iEEG (black) spectral profiles across vigilance states. The spectral overlap metric (numerical values) exceeded 0.5 in most frequency ranges, and the wake alpha peak was well recovered and appropriately diminished across sleep stages. By contrast, the hippocampus showed markedly lower spectral overlap between ViEEG and iEEG, especially in the delta and theta ranges, where ViEEG underestimated iEEG activity. During NREM sleep, overlap values in the hippocampus remained below 0.3 in all frequency bands, underscoring the limits of ViEEG for deep medial sources.

To more clearly contrast lateral and medial spectral estimation fidelity, we also compared the peak distributions (Fig. 5C-5D). In the middle temporal gyrus, both iEEG and ViEEG showed robust alpha peaks during wakefulness and stage R, along with visible delta peaks during NREM sleep. In contrast, the hippocampus showed low-frequency peak amplitudes in both modalities, with ViEEG systematically underestimating peak structure relative to iEEG, while also showing spurious overestimation of alpha peaks during wakefulness in lateral regions such as the middle temporal gyrus. These comparisons underscored the influence of cortical regions and depth on the accuracy of ViEEG source reconstructions, with lateral neocortical regions showing more reliable reconstruction than medial and deep structures.

4.4. Oscillatory peaks vary across the different vigilance states

When summarizing periodic peak properties within canonical frequency bands by comparing them with those observed in the MNI iEEG atlas across vigilance states in 38 regions, we found that oscillatory peaks vary across sleep stages (Fig. 6, Supplementary Figure 7-Figure 10 for all ROI specific findings). During wakefulness (Fig. 6A), both ViEEG and iEEG displayed prominent alpha-band peaks, though ViEEG overestimated the frontal alpha activity. In stage R (Fig. 6B), alpha peaks weakened and shifted toward slower frequencies, while variability in high beta increased, possibly due to lower signal-to-noise. During NREM sleep (Fig. 6C-6D), both modalities showed strong delta peaks, consistent with slow-wave dominance. Interesting, in N2, there was a peak around 13Hz in both ViEEG and iEEG in N2, while ViEEG exhibited the gamma peak in N3 sleep.

To quantify these differences at a regional level, we calculated the Peak estimation metric as a percentage difference that quantifies the overestimation or underestimation of HDEEG-estimated ViEEG channels showing oscillatory peaks when compared to ground-truth iEEG peaks (Figure 6E). Warmer colors indicate a higher proportion of channels exhibiting peaks compared to iEEG, and cooler colors indicate fewer detected peaks relative to the intracranial reference. ViEEG generally underestimated delta and theta peaks (<25%), particularly in posterior regions, though theta underestimation was minimal in REM and N2.

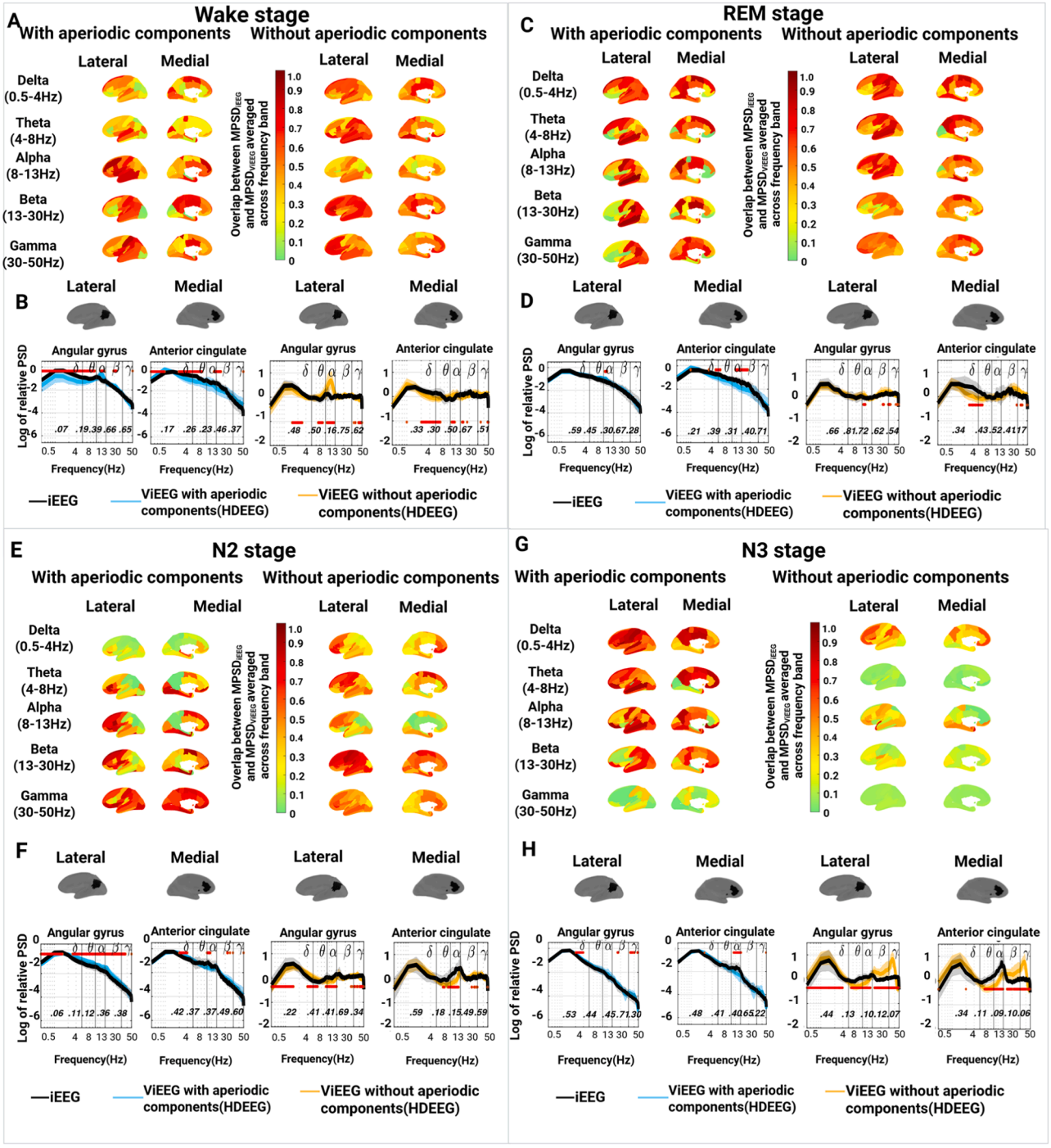

Fig. 4. Mean overlap between ViEEG and iEEG for 38 ROIs with and without aperiodic components across stage W, R, N2, and N3. (A, C, E, and G) Spectral overlap between ViEEG and iEEG across four sleep stages (Wake, R, N2, N3), before and after removal of aperiodic components using the FOOOF toolbox. Overlap was computed for each of the 38 ROIs using power spectra in five canonical frequency bands (delta, theta, alpha, beta, and gamma). The overlap value is calculated at each frequency bin and ranges from 0 to 1. For a ROI, if the median of PSD ViEEG perfectly coincides with the median of PSD iEEG at all frequency bins within a specific frequency band, the overlap is 1. The redder, the more overlap between iEEG and ViEEG. (B, D, F, and H) Comparison of periodic components of HDEEG-estimated spectra with ground truth iEEG, with aperiodic components (left) and without aperiodic components (right) shown for 2 ROIs (angular gyrus and anterior cingulate). For each spectrum, we are reporting the median value (black, light blue, and orange straight lines) together with the corresponding standard deviation (shaded area) over all channels. The frequency bins are marked as red dots when iEEG and ViEEG are statistically different (Mann-Whitney U Test, $p < 0.05$, multiple comparisons Bonferroni correction applied across 38 ROIs and 100 frequency bins). Abbreviations: ViEEG, virtual intracranial electroencephalography; iEEG, intracranial electroencephalography; ROI, region of interest; PSD, power spectral density; HDEEG, high-density electroencephalography; FOOOF, Fitting Oscillations and One-Over-F; W, Wake; R, REM (rapid eye movement sleep); N2/N3, non-rapid eye movement sleep stages 2 and 3.

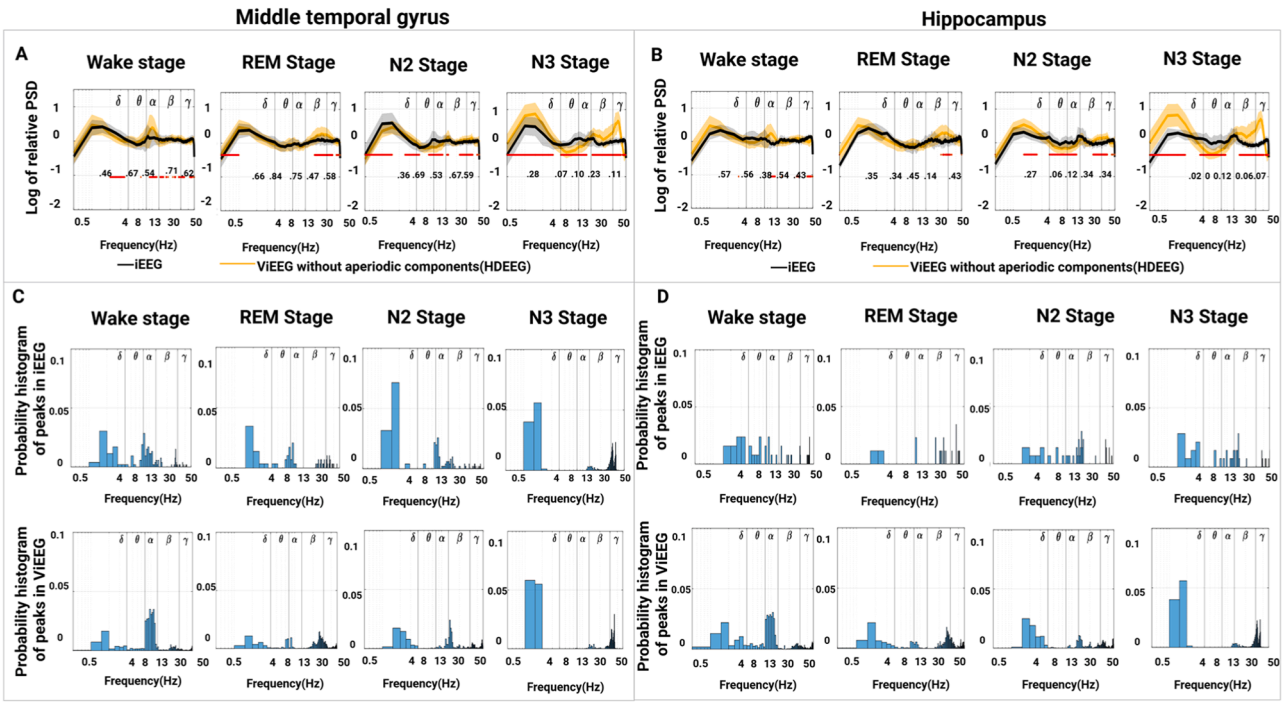

Fig. 5. Analysis of spectral oscillatory components (HDEEG) in the different sleep stages for the iEEG and ViEEG in the middle temporal gyrus and the hippocampus. Comparison of periodic components of HDEEG-estimated spectra with ground truth iEEG without aperiodic components shown for the middle temporal gyrus(A) and hippocampus(B). Power spectra are summarized by their median values across channels, shown as black (iEEG) and orange (ViEEG) curves, with shaded areas indicating the corresponding standard deviation at each frequency bin. In addition, a spectral overlap metric was computed at each frequency bin to quantify the similarity between ViEEG and iEEG power spectra. The frequency bins are marked as red dots when iEEG and ViEEG are statistically different (Mann-Whitney U Test, Bonferroni-corrected $p < 0.05$). C and D show the probability histogram of identified peaks in delta (0.5- 4Hz), theta (4- 8Hz), alpha (8- 13Hz), beta (13- 30Hz), and low gamma (30- 50Hz) in iEEG(top) and ViEEG(bottom). The probability histogram is calculated by the number of peaks in each bin divided by the total number of peaks in all bins. Abbreviations: HDEEG, high-density electroencephalography; iEEG, intracranial electroencephalography; ViEEG, virtual intracranial electroencephalography; PSD, power spectral density; W, Wake; R, REM (rapid eye movement sleep); N2/N3, non-rapid eye movement sleep stages 2 and 3; NROI, number of channels within a given region of interest.

Alpha peaks were substantially overestimated during wakefulness (>50%, especially frontally), underestimated during NREM sleep (<25%), and quietly concordant during the REM stage compared with iEEG. During REM sleep, beta-band peaks showed localized overestimation, mainly in opercular regions. Gamma-band peak overestimation was observed during N3 sleep and was primarily localized to frontal regions, with relative peak estimation differences exceeding 25% between ViEEG and iEEG.

4.5. HDEEG-derived ViEEG and MEG-derived ViEEG approximate iEEG spectral features

To further validate HDEEG source imaging, we applied the wMEM pipeline analysis for MEG-derived ViEEG data during wakefulness (Afnan et al., 2023). This allowed us to directly compare the ability of MEG and HDEEG to reconstruct cortical oscillatory activity relative to iEEG. Before aperiodic correction, both HDEEG- and MEG-derived ViEEG approximated iEEG power spectra across canonical bands (Fig. 7A), with good correspondence in delta, alpha, and beta frequencies. ViEEG from HDEEG exhibited more accurate spectral patterns in both lateral and medial views compared to MEG-derived ViEEG. Peak histograms revealed that MEG-derived ViEEG exhibited narrow distributions with sharp alpha-band peaks, whereas HDEEG-derived ViEEG showed broader peak distributions more similar to iEEG (Fig. 7B). Alpha-band peaks were substantially overestimated between HDEEG- and MEG-derived ViEEG when compared to iEEG data.

After removing the aperiodic background using FOOOF, both HDEEG- and MEG-derived ViEEG closely matched iEEG oscillatory components (Fig. 7C). By comparing HDEEG-derived ViEEG and MEG-derived ViEEG at the ROI level, HDEEG achieved a particularly close fit in lateral regions, while MEG showed a slightly stronger alignment in medial structures. These results highlight that both modalities can approximate iEEG spectral properties after appropriate preprocessing, with both providing good and complementary correspondence.

5. Discussion

Accurately localizing spontaneous cortical oscillations across sleep-wake states remains a central challenge. Although HDEEG with source imaging offers a noninvasive window into large-scale brain dynamics, its ability to resolve spatially distinct, frequency-specific patterns during natural sleep is still unclear. Moreover, how vigilance states modulate the noninvasive source estimates has not been systematically examined. Using HDEEG combined with the wMEM source localization method, we systematically assessed how well noninvasive source imaging captures cortical oscillations across sleep-wake states against the MNI iEEG atlas. We demonstrated that (i) HDEEG source imaging reliably captured comparable low-frequency spectral patterns but overestimated gamma activity across vigilance states, with better accuracy in lateral than medial cortical regions; (ii) Separating oscillatory from aperiodic components significantly improved spectral alignment between HDEEG-derived and iEEG signals, except for N3 sleep; and (iii) Oscillatory peak patterns in ViEEG reflected state-dependent dynamics that broadly align with iEEG peaks.

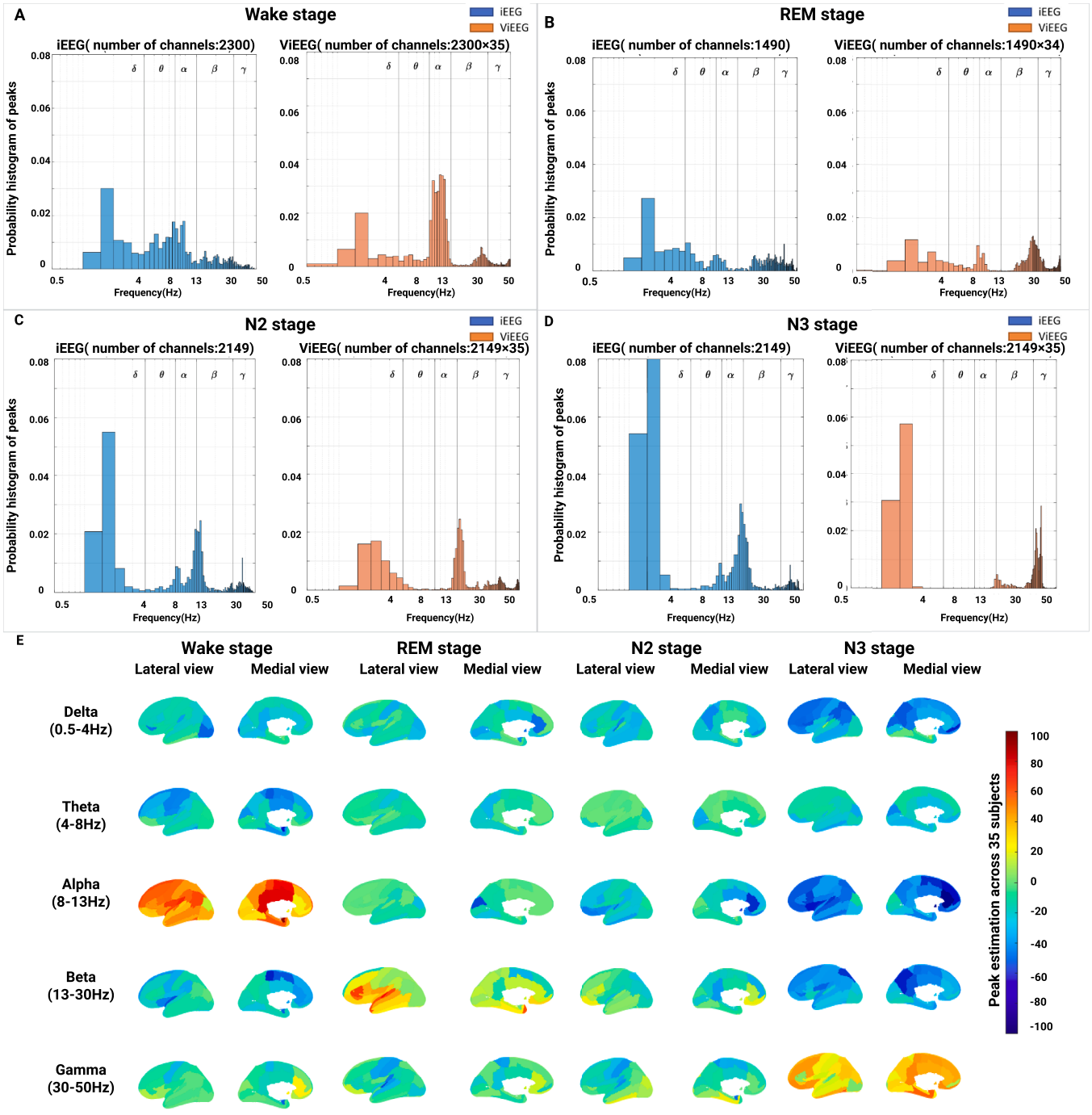

Fig. 6. Oscillatory Peak Dominance analysis between ViEEG and iEEG Across Vigilance States. (A)Probability histogram of all identified peaks in all ROIs for iEEG and ViEEG during wakefulness, The probability histogram is calculated by the number count of peaks in each bin divided by the total number count of peaks in all bins; (B) Probability histogram of all identified peaks in all ROIs for iEEG and ViEEG during stage R; (C) Probability histogram of all identified peaks in all ROIs for iEEG and ViEEG during N2 stage; (D) Probability histogram of all identified peaks in all ROIs for iEEG and ViEEG during N3 stage. (E) Peak estimation matrix calculated by HDEEG in all spectral bands compared to iEEG across vigilance states. The plotted values represent the group-level median of Peak_estimated across 35 subjects, ranging from −100% (complete underestimation) to +100% (complete overestimation). Abbreviations: ViEEG, virtual intracranial electroencephalography; iEEG, intracranial electroencephalography; ROI, region of interest; HDEEG, high-density electroencephalography; REM, rapid eye movement; N2/N3, non-rapid eye movement sleep stages 2 and 3; Peak_estimated, percentage difference in number of oscillatory peaks in ViEEG relative to iEEG.

5.1. Spectral concordance and discrepancies revealed by HDEEG source imaging

Validating whether noninvasive source imaging can recover cortical oscillation dynamics across sleep stages is crucial for advancing EEG-based brain mapping. Our findings demonstrated that ViEEG, derived from high-density scalp EEG wMEM source estimates, can reliably approximate spatial spectral patterns observed in iEEG in the low-frequency (delta, theta, and alpha) bands during wakefulness and sleep, which are consistent with previous studies (Fan et al., 2023, Kalamangalam et al., 2021, Brancaccio et al., 2020). In contrast, ViEEG did not reliably capture gamma-band activity across vigilance states, showing notable discrepancies likely due to contamination from muscle artifacts and movement-related noise (Murphy et al., 2009,

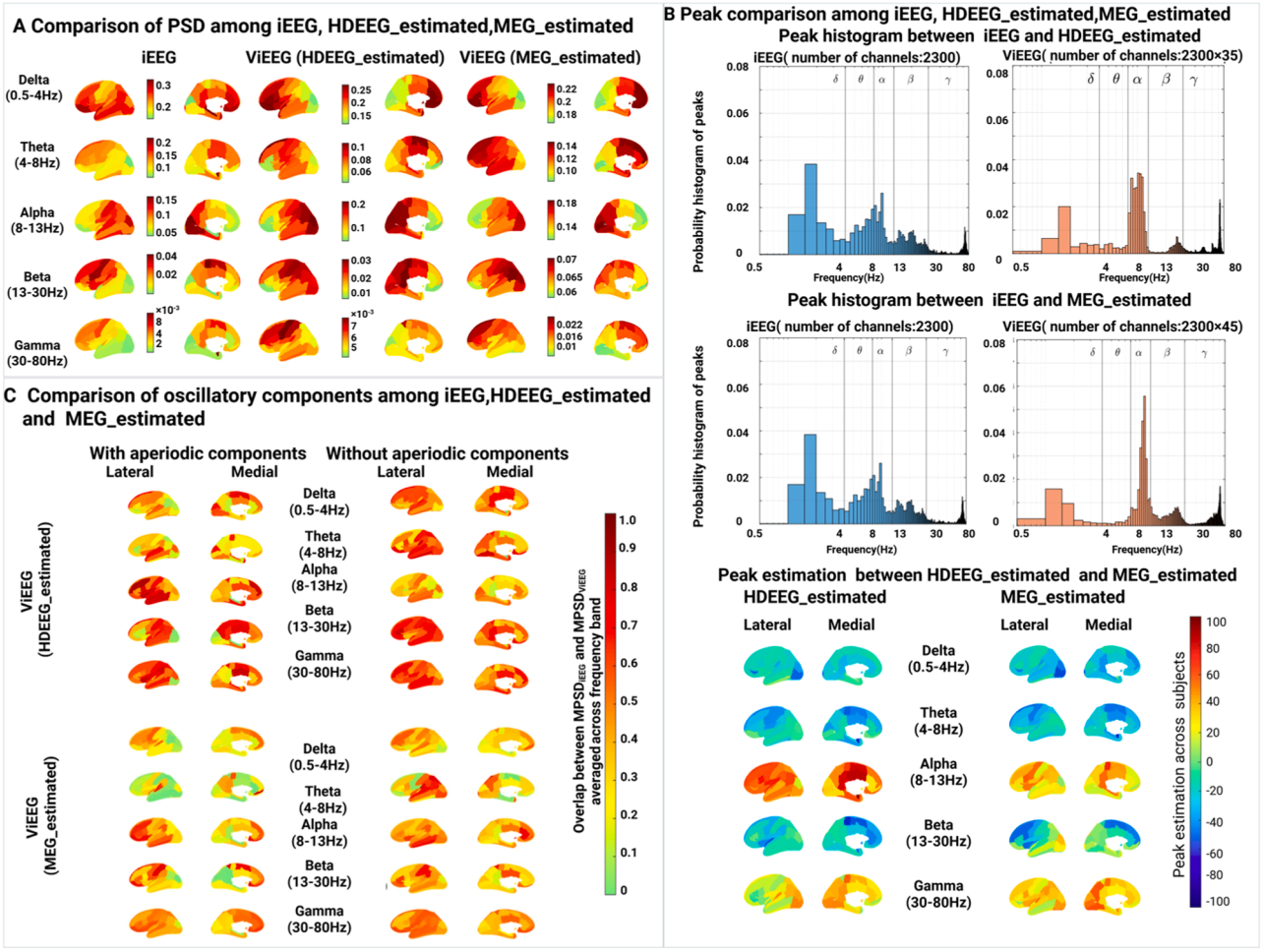

Fig. 7. Comparison among iEEG, ViEEG (HDEEG_estimated), and ViEEG (MEG_estimated) in terms of spectral power, oscillatory components, and peak distributions during wakefulness. (A)Relative power spectral density (PSD) maps across five canonical frequency bands (delta, theta, alpha, beta, gamma) are shown for iEEG, ViEEG estimated from HDEEG, and ViEEG estimated from MEG. Color bars are modality-specific. (B) Top: Probability histograms of all identified oscillatory peaks in 38 ROIs for iEEG, HDEEG-based ViEEG, and MEG-based ViEEG. Bottom: Spatial distribution of median Peak_estimated values across 35 subjects, values range from −100% to 100%. (C) Comparison of oscillatory components among modalities, with and without the aperiodic background (fitted using FOOOF). Overlap was computed for each of the 38 ROIs using power spectra in five canonical frequency bands (delta, theta, alpha, beta, and gamma). The overlap value is calculated at each frequency bin and ranges from 0 to 1. Abbreviations: iEEG, intracranial electroencephalography; ViEEG, virtual intracranial electroencephalography; HDEEG, high-density electroencephalography; MEG, magnetoencephalography; PSD, power spectral density; ROI, region of interest; FOOOF, Fitting Oscillations and One-Over-F; Peak_estimation, percentage difference in the number of oscillatory peaks between ViEEG and iEEG.

Muthukumaraswamy, 2013). Stage R sleep, characterized by minimal muscle tone, appeared more consistent. Additionally, gamma-band profiles in stage N3 diverged from those in stage N2, potentially reflecting relatively lower high-frequency neural activity during deep sleep. These findings underscore that gamma-band interpretations from surface EEG require caution and "stage-specific" consideration. Additionally, the HDEEG estimated relative power was spatially more smoothly distributed compared to the MNI iEEG atlas, which is consistent with our previous work (Afnan et al., 2023). Explicitly, the iEEG data displayed clear differences, a broader range of activity from strongest to weakest among ROIs, whereas the ViEEG displayed more consistent activation across neighboring ROIs, covering a narrower range of activity.

5.2. *Aperiodic component removal improves spectral alignment*

Disentangling periodic and aperiodic components is essential for accurate interpretation of EEG spectral features, particularly across varying brain states. Electrophysiological power spectra consist of both oscillatory rhythms and non-oscillatory aperiodic activity, also referred to as scale-free or 1/f-like background (He, 2014). We applied the FOOOF (Donoghue et al., 2020) to separate the periodic and aperiodic parts of the spectrum. After aperiodic removal, the ViEEG spectral power became more comparable to iEEG across all frequency bands during Wake, REM, and N2 stages. The spectral differences between ViEEG and iEEG are largely driven by variations in aperiodic components, likely reflecting spatial interactions among synchronized neurons (Mazzetti and Carbone, 2022, Abbas, 2019). iEEG records brain activity locally with a spatial sensitivity of less than 1 cm (Parvizi and Kastner, 2018), while HDEEG has a broader spatial sensitivity (Mégevand and Electroencephalography, 2018, Michel and Brunet, 2019). Interestingly, the N3 sleep was the only stage where overlap values decreased. Discrepancies in N3 likely suggest that aperiodic activity contributes differentially across sleep stages and may interfere with spectral alignment in deeper sleep due to the significant amount of slow sleep waves, FOOOF's reduced accuracy under low signal-to-noise conditions (Donoghue et al., 2020, Gerster et al., 2022).

5.3. *Reduced accuracy in medial structures highlights spatial constraints*

Evaluating how spatial location affects ViEEG accuracy is critical for understanding the limits of noninvasive source modeling. We found that

HDEEG-derived ViEEG performed better in lateral cortical regions than in medial structures. After removal of the aperiodic components, spectral overlap values in lateral regions frequently exceeded 0.5, while medial areas such as the hippocampus showed limited improvement and ranged below 0.5. This spatial discrepancy aligns with known limitations of scalp EEG source imaging, which favors superficial sources and is prone to signal attenuation and spatial smearing at greater depths (Michel and Brunet, 2019, Zorzos et al., 2021), Even if depth weighting was added within our MEM framework to improve sensitivity to deep structure (Afnan et al., 2024), localizing brain activity in deep regions remains challenging, notably when considering low SNR resting state data. Supporting this, simultaneous scalp-iEEG studies have shown that seizures originating from mesial temporal structures often lack clear scalp correlates (Barborica et al., 2021), and localization accuracy is markedly reduced for deep generators (Ramantani et al., 2016).

5.4. Oscillatory peak patterns reflect state-dependent differences

Analyzing spectral peak frequencies provides complementary insight into how well ViEEG captures the dominant rhythms of brain activity across vigilance states. We observed broadly similar peak distributions between iEEG and ViEEG with state-dependent differences. During wakefulness and stage R sleep, both modalities exhibited alpha-band peaks (8–13 Hz), but ViEEG overestimated alpha power. As reported by (Srinivasan et al., 2006), alpha activity becomes more widespread with eyes closed, potentially contributing to the observed overestimation of alpha peaks in frontal regions. Alpha in deep regions may reflect cortical leakage, as also seen in scalp studies (Afnan et al., 2023, Srinivasan et al., 2006). Notably, iEEG studies have shown that intrinsic dominant frequencies often lie closer to ~7 Hz (theta range), not the classical alpha band (Groppe et al., 2013). In REM, ViEEG also overestimated beta peaks in anterior regions, potentially reflecting increased beta phase synchronization (Ferri et al., 2001, Uchida et al., 1992). During NREM sleep, iEEG showed delta and theta peaks in frontotemporal regions. This aligns with the known increase in delta activity during deeper sleep (Dijk, 2009, Felice et al., 2013, Ioannides et al., 2017). A gradual underestimation from N2 to N3 in the alpha and beta bands is consistent with suppression of alpha band activity in N3 (Benca et al., 1999) and systematic decrease of beta from light to deep sleep (Armitage, 1995). A spectral peak near 13 Hz, likely corresponding to sleep spindle activity, was observed in both ViEEG and iEEG during N2 sleep and to a lesser extent in N3, consistent with previous studies reporting spindle-related activity predominantly in N2 but occasionally persisting into early N3 stages (Purcell et al., 2017). In contrast, ViEEG overestimated gamma peaks in N3, likely driven by limitations in spectral fitting by FOOOF (Tiwari et al., 2023).

5.5. HDEEG and MEG show complementary spectral correspondence with iEEG

Comparing noninvasive modalities provides insight into their complementary capacities for reconstructing cortical oscillations. In this context, we reanalyzed MEG data reported (Afnan et al., 2023) using the depth-weighted extension of wMEM (Afnan et al., 2024). This harmonized approach ensured that observed differences primarily reflected intrinsic modality characteristics. Both HDEEG- and MEG-derived ViEEG demonstrated convergent spectral correspondence with iEEG, particularly in the delta, alpha, and beta bands, which correspond to previous works (Seeber et al., 2019, Baillet, 2017). After removing the aperiodic signal using FOOOF, both modalities improved their correspondence with the iEEG oscillatory patterns. At the same time, there are subtle differences; HDEEG more consistently reflected oscillatory patterns broadly, whereas MEG provided complementary information more specifically. This difference may reflect underlying differences in the aperiodic component between EEG and MEG. Prior studies have shown that EEG and iEEG exhibit more similar 1/f scaling properties than MEG (Bénar et al., 2019), which likely facilitates more accurate oscillatory estimation in EEG-based ViEEG. These findings highlight the importance of accounting for modality-specific 1/f structure when comparing spectral estimates, and support the use of FOOOF or similar tools to improve cross-modality alignment.

5.6. Strengths and limitations

This study systematically provides a direct cross-modal comparison between noninvasive HDEEG source imaging and a large-scale normative intracranial EEG (iEEG) atlas across 5 frequency bands, 38 regions, and 4 vigilance states. Our findings highlight the capacity of HDEEG to capture state-dependent cortical oscillations, with improved alignment after aperiodic signal removal, offering a robust framework for noninvasive investigations of human sleep neurophysiology. In parallel, we acknowledge some limitations. A general and unavoidable limitation is that iEEG recordings come from patients with epilepsy, where both the disease and antiseizure medications may influence sleep-related brain signals. We mitigated this by analyzing electrodes in healthy regions. HDEEG recordings are also susceptible to artifacts during sleep; we minimized this through strict acquisition protocols and preprocessing. In addition, subcortical structures remain difficult to localize using scalp EEG, although wMEM shows the utility for capturing spontaneous cortical activities. More advanced biophysical models of deep sources (e.g., hippocampus, thalamus) may aid in recovering deep, low-SNR activity.

Additionally, we note that hemispheric differences were not explicitly examined in the present analysis. Our spectral overlap values were computed at the regional level by aggregating homologous regions across hemispheres, an approach chosen to enable robust statistical comparisons and direct alignment with the normative iEEG atlas framework. Potential hemispheric asymmetries in cortical oscillatory organization were not assessed; future studies incorporating hemisphere-specific analyses and larger datasets may provide additional insights into lateralized differences in cortical oscillations across vigilance states. Finally, the discrepancy in N3 sleep (decreased overlap value and overestimated gamma peaks) may show the limitation of the FOOOF-based spectral decomposition, likely due to flatter spectra and weaker oscillatory peaks in deep sleep, which challenge the oscillatory peaks. Emerging alternatives may offer more robust approaches to disentangle periodic and aperiodic activity under such conditions.

6. Conclusion

In this study, we provide evidence that HDEEG source imaging reliably captures state-dependent cortical oscillations across the sleep-wake cycle. The reconstructed spectral profiles from HDEEG align well with iEEG patterns in low-frequency bands and lateral regions and show improved correspondence after removal of aperiodic signal components. These findings reveal that vigilance states substantially modulate the spatial and spectral features of noninvasive source imaging and support the use of HDEEG as a powerful tool for mapping human brain dynamics during natural sleep.

Data and code availability statement

The normative intracranial EEG (iEEG) atlas from 110 epilepsy patients with electrodes in healthy brain regions is publicly shared in (https://mni-open-ieegatlas.research.mcgill.ca/). The HDEEG overnight recordings (Wei et al., 2024) are available through (https://doi.org/10.17605/OSF.IO/R26FH). HDEEG and iEEG data were analyzed in the Brainstorm (Tadel et al., 2011) software package, implemented in MATLAB (MathWorks, Natick, MA). The wMEM method is available within the Brain Entropy in space and time (Best) plugin of Brainstorm software(https://neuroimage.usc.edu/brainstorm/Tutorials/TutBEst). Power spectrum parameterization with the FOOOF toolbox (Donoghue

et al., 2020) was performed via the corresponding MATLAB wrapper (https://github.com/fooof-tools/fooof_mat).

Funding

This work was supported by project grants from the Canadian Institutes of Health Research (PJT-175056 to B.F., PJT-159448 and PJT-195828 to C.G.) and the Natural Sciences and Engineering Research Council of Canada (RGPIN-2020-04127 and RGPAS-2020-00021 to B.F.; RGPIN-2018-06707 and RGPIN-2025-06816 to C.G.).

CRediT authorship contribution statement

Xiaoyan Wei: Writing – review & editing, Writing – original draft, Visualization, Validation, Software, Resources, Project administration, Methodology, Investigation, Formal analysis, Data curation, Conceptualization. **Jawata Afnan:** Writing – review & editing, Visualization, Validation, Software, Methodology, Investigation, Formal analysis, Data curation. **Tamir Avigdor:** Writing – review & editing, Visualization, Validation, Software, Methodology, Investigation, Data curation, Conceptualization. **Nicolás von Ellenrieder:** Writing – review & editing, Validation, Methodology, Investigation, Data curation. **Édouard Delaire:** Writing – review & editing, Software, Methodology, Data curation. **Jessica Royer:** Writing – review & editing, Software, Resources, Data curation. **Alyssa Ho:** Writing – review & editing, Software, Resources, Data curation. **Erica Minato:** Writing – review & editing, Resources, Data curation. **Katharina Schiller:** Writing – review & editing, Resources, Investigation, Data curation. **Kassem Jaber:** Writing – review & editing, Resources, Data curation. **Yingqi Laetitia Wang:** Writing – review & editing, Resources, Data curation. **Matt Moye:** Writing – review & editing, Project administration, Data curation. **Boris C Bernhardt:** Writing – review & editing, Resources, Data curation. **Jean-Marc Lina:** Writing – review & editing, Validation, Software, Methodology. **Christophe Grova:** Writing – review & editing, Visualization, Validation, Supervision, Resources, Methodology, Funding acquisition, Formal analysis, Conceptualization. **Birgit Frauscher:** Writing – review & editing, Visualization, Validation, Supervision, Software, Resources, Project administration, Methodology, Investigation, Funding acquisition, Formal analysis, Data curation, Conceptualization.

Declaration of competing interest

The authors declare that they have no known competing financial interests or personal relationships that could have appeared to influence the work reported in this paper.

Acknowledgements

We wish to express our appreciation to the clinical and research EEG technicians at the EEG Department of the Montreal Neurological Institute and Hospital, particularly Lorraine Allard, Chantal Lessard, Jessica Brisebois, and Monica Wang.

Supplementary materials

Supplementary material associated with this article can be found, in the online version, at doi:10.1016/j.neuroimage.2026.121803.

References

Abbas A. Understanding Brain Activity Dynamics through the Investigation of Quasi-Periodic Patterns. 2019. https://www.proquest.com/docview/2354085417/abstract/A40D641559954F17PQ/1. Accessed March 2, 2025.

Abdallah, C., Hedrich, T., Koupparis, A., et al., 2022. Clinical Yield of Electromagnetic Source Imaging and Hemodynamic Responses in Epilepsy. Neurology 98 (24), e2499–e2511. https://doi.org/10.1212/WNL.0000000000200337.

Acar, Z.A., Acar, C.E., Makeig, S., 2016. Simultaneous head tissue conductivity and EEG source location estimation. Neuroimage 124 (0 0), 168–180. https://doi.org/10.1016/j.neuroimage.2015.08.032.

Afnan, J., von Ellenrieder, N., Lina, J.M., et al., 2023. Validating MEG source imaging of resting state oscillatory patterns with an intracranial EEG atlas. NeuroImage 274, 120158. https://doi.org/10.1016/j.neuroimage.2023.120158.

Afnan, J., Cai, Z., Lina, J., et al., 2024. EEG/MEG source imaging of deep brain activity within the maximum entropy on the mean framework: simulations and validation in epilepsy. Hum. Brain Mapp. 45 (10), e26720. https://doi.org/10.1002/hbm.26720.

Afnan, J., Cai, Z., Lina, J.M., et al., 2025. Validating MEG estimated resting-state connectome with intracranial EEG. Netw. Neurosci. 9 (1), 421–446. https://doi.org/10.1162/netn_a_00441.

Amblard, C., Lapalme, E., Lina, JM., 2004. Biomagnetic source detection by maximum entropy and graphical models. IEEE Trans. Biomed. Eng. 51 (3), 427–442. https://doi.org/10.1109/TBME.2003.820999.

Armitage, R., 1995. The Distribution of EEG Frequencies in REM and NREM Sleep Stages in Healthy Young Adults. Sleep 18 (5), 334–341. https://doi.org/10.1093/sleep/18.5.334.

Avigdor, T., Abdallah, C., von Ellenrieder, N., et al., 2021. Fast oscillations >40 Hz localize the epileptogenic zone: an electrical source imaging study using high-density electroencephalography. Clin. Neurophysiol. 132 (2), 568–580. https://doi.org/10.1016/j.clinph.2020.11.031.

Avigdor, T., Abdallah, C., Afnan, J., et al., 2024. Consistency of electrical source imaging in presurgical evaluation of epilepsy across different vigilance states. Ann. Clin. Transl. Neurol. 11 (2), 389–403. https://doi.org/10.1002/acn3.51959.

Aydin, Ü, Pellegrino, G., Ali, O.B.K., et al., 2020. Magnetoencephalography resting state connectivity patterns as indicatives of surgical outcome in epilepsy patients. J. Neural. Eng. 17 (3), 035007. https://doi.org/10.1088/1741-2552/ab8113.

Bénar, C.G., Grova, C., Jirsa, V., Lina, J., 2019. Differences in MEG and EEG power-law scaling explained by a coupling between spatial coherence and frequency: a simulation study. J. Comput. Neurosci. 47 (1), 31–41. https://doi.org/10.1007/s10827-019-00721-9.

Baillet, S., 2017. Magnetoencephalography for brain electrophysiology and imaging. Nat. Neurosci. 20 (3), 327–339. https://doi.org/10.1038/nn.4504.

Barborica, A., Mindruta, I., Sheybani, L., et al., 2021. Extracting seizure onset from surface EEG with independent component analysis: insights from simultaneous scalp and intracerebral EEG. Neuroimage Clin 32, 102838. https://doi.org/10.1016/j.nicl.2021.102838.

Benca, R.M., Obermeyer, W.H., Larson, C.L., et al., 1999. EEG alpha power and alpha power asymmetry in sleep and wakefulness. Psychophysiology 36 (4), 430–436. https://doi.org/10.1111/1469-8986.3640430.

Brancaccio, A., Tabarelli, D., Bigica, M., Baldauf, D., 2020. Cortical source localization of sleep-stage specific oscillatory activity. Sci. Rep. 10, 6976. https://doi.org/10.1038/s41598-020-63933-5.

Buzsáki, G., Draguhn, A., 2004. Neuronal oscillations in cortical networks. Science 304 (5679), 1926–1929. https://doi.org/10.1126/science.1099745.

Cai, Z., Sohrabpour, A., Jiang, H., et al., 2021. Noninvasive high-frequency oscillations riding spikes delineates epileptogenic sources. Proc. Natl. Acad. Sci. 118 (17), e2011130118. https://doi.org/10.1073/pnas.2011130118.

Cao, M., Galvis, D., Vogrin, S.J., et al., 2022. Virtual intracranial EEG signals reconstructed from MEG with potential for epilepsy surgery. Nat. Commun. 13 (1), 994. https://doi.org/10.1038/s41467-022-28640-x.

Chowdhury, R.A., Lina, J.M., Kobayashi, E., Grova, C., 2013. MEG source localization of spatially extended generators of epileptic activity: comparing entropic and hierarchical bayesian approaches. PLOS ONE 8 (2), e55969. https://doi.org/10.1371/journal.pone.0055969.

Chowdhury, R.A., Merlet, I., Birot, G., et al., 2016. Complex patterns of spatially extended generators of epileptic activity: Comparison of source localization methods cMEM and 4-ExSo-MUSIC on high resolution EEG and MEG data. NeuroImage 143, 175–195. https://doi.org/10.1016/j.neuroimage.2016.08.044.

Collins, D.L., Neelin, P., Peters, T.M., Evans, AC., 1994. Automatic 3D intersubject registration of MR volumetric data in standardized Talairach space. J. Comput. Assist. Tomogr. 18 (2), 192.

Cruces, R.R., Royer, J., Herholz, P., et al., 2022. Micapipe: A pipeline for multimodal neuroimaging and connectome analysis. NeuroImage 263, 119612. https://doi.org/10.1016/j.neuroimage.2022.119612.

Dijk, DJ., 2009. Regulation and functional correlates of slow wave sleep. J. Clin. Sleep Med. 5 (2 suppl), S6–S15. https://doi.org/10.5664/jcsm.5.2S.S6.

Donoghue, T., Haller, M., Peterson, E.J., et al., 2020. Parameterizing neural power spectra into periodic and aperiodic components. Nat. Neurosci. 23 (12), 1655–1665. https://doi.org/10.1038/s41593-020-00744-x.

Fan, J.M., Kudo, K., Verma, P., et al., 2023. Cortical synchrony and information flow during transition from wakefulness to light non-rapid eye movement sleep. J. Neurosci. 43 (48), 8157–8171. https://doi.org/10.1523/JNEUROSCI.0197-23.2023.

Felice, A.D., Arcaro, C., Storti, S.F., Fiaschi, A., Manganotti, P., 2013. Electrical source imaging of sleep spindles. Clin. EEG Neurosci. https://doi.org/10.1177/1550059413497716. October.

Ferri, R., Cosentino, F.I.I., Elia, M., Musumeci, S.A., Marinig, R., Bergonzi, P., 2001. Relationship between Delta, Sigma, Beta, and Gamma EEG bands at REM sleep onset and REM sleep end. Clin. Neurophysiol. 112 (11), 2046–2052. https://doi.org/10.1016/S1388-2457(01)00656-3.

Frauscher, B., Von Ellenrieder, N., Zelmann, R., et al., 2018. Atlas of the normal intracranial electroencephalogram: neurophysiological awake activity in different cortical areas. Brain 141 (4), 1130–1144. https://doi.org/10.1093/brain/awy035.

Frauscher, B., von Ellenrieder, N., Zelmann, R., et al., 2018. Atlas of the normal intracranial electroencephalogram: neurophysiological awake activity in different cortical areas. Brain 141 (4), 1130–1144. https://doi.org/10.1093/brain/awy035.
Gerster, M., Waterstraat, G., Litvak, V., et al., 2022. Separating neural oscillations from aperiodic 1/f activity: challenges and recommendations. Neuroinform 20 (4), 991–1012. https://doi.org/10.1007/s12021-022-09581-8.
Gramfort, A., Papadopoulo, T., Olivi, E., Clerc, M., 2010. OpenMEEG: opensource software for quasistatic bioelectromagnetics. Biomed. Eng. Online 9, 45. https://doi.org/10.1186/1475-925X-9-45.
Groppe, D.M., Bickel, S., Keller, C.J., et al., 2013. Dominant frequencies of resting human brain activity as measured by the electrocorticogram. NeuroImage 79, 223–233. https://doi.org/10.1016/j.neuroimage.2013.04.044.
Grova, C., Aiguabella, M., Zelmann, R., Lina, J.M., Hall, J.A., Kobayashi, E., 2016. Intracranial EEG potentials estimated from MEG sources: a new approach to correlate MEG and iEEG data in epilepsy. Hum. Brain Mapp. 37 (5), 1661–1683. https://doi.org/10.1002/hbm.23127.
He, B., Sohrabpour, A., Brown, E., Liu, Z., 2018. Electrophysiological source imaging: a noninvasive window to brain dynamics. Annu. Rev. Biomed. Eng. 20, 171–196. https://doi.org/10.1146/annurev-bioeng-062117-120853.
He, BJ., 2014. Scale-free brain activity: past, present, and future. Trends Cogn. Sci. 18 (9), 480–487. https://doi.org/10.1016/j.tics.2014.04.003.
Hedrich, T., Pellegrino, G., Kobayashi, E., Lina, J.M., Grova, C., 2017. Comparison of the spatial resolution of source imaging techniques in high-density EEG and MEG. NeuroImage 157, 531–544. https://doi.org/10.1016/j.neuroimage.2017.06.022.
Herweg, N.A., Solomon, E.A., Kahana, MJ., 2020. Theta oscillations in human memory. Trends Cogn. Sci. 24 (3), 208–227. https://doi.org/10.1016/j.tics.2019.12.006.
Ioannides, A.A., Liu, L., Poghosyan, V., Kostopoulos, GK., 2017. Using MEG to understand the progression of light sleep and the emergence and functional roles of spindles and k-complexes. Front. Hum. Neurosci. 11. https://doi.org/10.3389/fnhum.2017.00313.
Kalamangalam, G.P., Long, S., Chelaru, MI., 2021. Neurophysiological brain mapping of human sleep-wake states. Clin. Neurophysiol. 132 (7), 1550–1563. https://doi.org/10.1016/j.clinph.2021.03.014.
Kreidenhuber, R., De Tiège, X., Rampp, S., 2019. Presurgical functional cortical mapping using electromagnetic source imaging. Front Neurol. 10. https://doi.org/10.3389/fneur.2019.00628.
Landman, BA, Warfield, SK (Eds.), 2012. Create Space Independent Publishing Platform.
Lina, J.M., Chowdhury, R., Lemay, E., Kobayashi, E., Grova, C., 2014. Wavelet-based localization of oscillatory sources from magnetoencephalography data. IEEE Trans. Biomed. Eng. 61 (8), 2350–2364. https://doi.org/10.1109/TBME.2012.2189883.
Lina, J.M., Chowdhury, R., Lemay, E., Kobayashi, E., Grova, C., 2014. Wavelet-based localization of oscillatory sources from magnetoencephalography data. IEEE Trans. Biomed. Eng. 61 (8), 2350–2364. https://doi.org/10.1109/TBME.2012.2189883.
Lustenberger, C., Huber, R., 2012. High density electroencephalography in sleep research: potential, problems, future perspective. Front Neurol. 3, 77. https://doi.org/10.3389/fneur.2012.00077.
Mégevand, P., Electroencephalography, Seeck M., 2018. magnetoencephalography and source localization: their value in epilepsy. Curr. Opin. Neurol. 31 (2), 176. https://doi.org/10.1097/WCO.0000000000000545.
Mattout, J., Pélégrini-Issac, M., Garnero, L., Benali, H., 2005. Multivariate source prelocalization (MSP): use of functionally informed basis functions for better conditioning the MEG inverse problem. NeuroImage 26 (2), 356–373. https://doi.org/10.1016/j.neuroimage.2005.01.026.
Mazzetti, P., Carbone, A., 2022. Periodic and non-periodic brainwaves emerging via stochastic Syncronization of closed loops of firing neurons. Algorithms 15 (11), 396. https://doi.org/10.3390/a15110396.
Michel, C.M., Brunet, D., 2019. EEG source imaging: a practical review of the analysis steps. Front. Neurol. 10, 325. https://doi.org/10.3389/fneur.2019.00325.
Michel, C.M., He, B., 2019. Chapter 6 - EEG source localization. In: Levin, K.H., Chauvel, P. (Eds.), *Handbook of Clinical Neurology*. Vol 160. Clinical Neurophysiology: Basis and Technical Aspects. Elsevier, pp. 85–101. https://doi.org/10.1016/B978-0-444-64032-1.00006-0.
Murphy, M., Riedner, B.A., Huber, R., Massimini, M., Ferrarelli, F., Tononi, G., 2009. Source modeling sleep slow waves. Proc. Natl. Acad. Sci. 106 (5), 1608–1613. https://doi.org/10.1073/pnas.0807933106.
Muthukumaraswamy, SD., 2013. High-frequency brain activity and muscle artifacts in MEG/EEG: a review and recommendations. Front. Hum. Neurosci. 7, 138. https://doi.org/10.3389/fnhum.2013.00138.
Myrov, V., Siebenhühner, F., Juvonen, J.J., Arnulfo, G., Palva, S., Palva, JM., 2024. Rhythmicity of neuronal oscillations delineates their cortical and spectral architecture. Commun. Biol. 7 (1), 405. https://doi.org/10.1038/s42003-024-06083-y.
Parvizi, J., Kastner, S., 2018. Promises and limitations of human intracranial electroencephalography. Nat. Neurosci. 21 (4), 474–483. https://doi.org/10.1038/s41593-018-0108-2.
Pellegrino, G., Hedrich, T., Chowdhury, R., et al., 2016. Source localization of the seizure onset zone from ictal EEG/MEG data. Hum. Brain Mapp. 37 (7), 2528–2546. https://doi.org/10.1002/hbm.23191.
Pellegrino, G., Hedrich, T., Porras-Bettancourt, M., et al., 2020. Accuracy and spatial properties of distributed magnetic source imaging techniques in the investigation of focal epilepsy patients. Hum. Brain Mapp. 41 (11), 3019–3033. https://doi.org/10.1002/hbm.24994.
Pigorini, A., Mikulan, E., Russo, S., et al., 2023. Loss of differentiation and complexity in the sleeping human brain: a multi-scale analysis. Brain Stimul.: Basic Transl. Clin. Res. Neuromodulation 16 (1), 254. https://doi.org/10.1016/j.brs.2023.01.412.
Pizzo, F., Roehri, N., Medina Villalon, S., et al., 2019. Deep brain activities can be detected with magnetoencephalography. Nat. Commun. 10, 971. https://doi.org/10.1038/s41467-019-08665-5.
Prichard, D., Theiler, J., 1994. Generating surrogate data for time series with several simultaneously measured variables. Phys. Rev. Lett. 73 (7), 951–954. https://doi.org/10.1103/PhysRevLett.73.951.
Purcell, S.M., Manoach, D.S., Demanuele, C., et al., 2017. Characterizing sleep spindles in 11,630 individuals from the National Sleep Research Resource. Nat. Commun. 8, 15930. https://doi.org/10.1038/ncomms15930.
Quintiliani, M., Bianchi, F., Fuggetta, F., et al., 2021. Role of high-density EEG (hdEEG) in pre-surgical epilepsy evaluation in children: case report and review of the literature. Childs Nerv Syst 37 (5), 1429–1437. https://doi.org/10.1007/s00381-021-05069-z.
Ramantani, G., Maillard, L., Koessler, L., 2016. Correlation of invasive EEG and scalp EEG. Seizure 41, 196–200. https://doi.org/10.1016/j.seizure.2016.05.018.
Seeber, M., Cantonas, L.M., Hoevels, M., Sesia, T., Visser-Vandewalle, V., Michel, CM., 2019. Subcortical electrophysiological activity is detectable with high-density EEG source imaging. Nat. Commun. 10 (1), 753. https://doi.org/10.1038/s41467-019-08725-w.
Sohrabpour, A., Cai, Z., Ye, S., Brinkmann, B., Worrell, G., He, B., 2020. Noninvasive electromagnetic source imaging of spatiotemporally distributed epileptogenic brain sources. Nat. Commun. 11 (1), 1946. https://doi.org/10.1038/s41467-020-15781-0.
Srinivasan, R., Winter, W.R., Nunez, PL., 2006. Source analysis of EEG oscillations using high-resolution EEG and MEG. In: Neuper, C., Klimesch, W. (Eds.), *Progress in Brain Research*. Vol 159. Event-Related Dynamics of Brain Oscillations. Elsevier, pp. 29–42. https://doi.org/10.1016/S0079-6123(06)59003-X.
Taberna, G.A., Samogin, J., Zhao, M., et al., 2024. Large-scale analysis of neural activity and connectivity from high-density electroencephalographic data. Comput. Biol. Med. 178, 108704. https://doi.org/10.1016/j.compbiomed.2024.108704.
Tadel, F., Baillet, S., Mosher, J.C., Pantazis, D., Leahy, RM., 2011. Brainstorm: a user-friendly application for MEG/EEG analysis. Comput. Intell. Neurosci., 879716 https://doi.org/10.1155/2011/879716, 2011.
Taylor, P.N., Papasavvas, C.A., Owen, T.W., et al., 2022. Normative brain mapping of interictal intracranial EEG to localize epileptogenic tissue. Brain 145 (3), 939–949. https://doi.org/10.1093/brain/awab380.
Tiwari, A., Wu, G., Innanen, K., Mahnam, A., Moineau, B., Falk, TH., 2023. On the Use of FOOOF for electroencephalography quality measurement and device assessment. In: 2023 IEEE International Conference on Systems, Man, and Cybernetics (SMC), pp. 4746–4751. https://doi.org/10.1109/SMC53992.2023.10394590.
Uchida, S., Maloney, T., Feinberg, I., 1992. Beta (20–28 Hz) and Delta (0.3–3 Hz) EEGs oscillate reciprocally across NREM and REM Sleep. Sleep 15 (4), 352–358. https://doi.org/10.1093/sleep/15.4.352.
Uusitalo, M.A., Ilmoniemi, RJ., 1997. Signal-space projection method for separating MEG or EEG into components. Med. Biol. Eng. Comput. 35 (2), 135–140. https://doi.org/10.1007/BF02534144.
von Ellenrieder, N., Pellegrino, G., Hedrich, T., et al., 2016. Detection and magnetic source imaging of fast oscillations (40–160 Hz) recorded with magnetoencephalography in focal epilepsy patients. Brain Topogr. 29, 218–231. https://doi.org/10.1007/s10548-016-0471-9.
Von Ellenrieder, N., Gotman, J., Zelmann, R., et al., 2020. How the Human Brain Sleeps: direct Cortical Recordings of Normal Brain Activity. Ann. Neurol. 87 (2), 289–301. https://doi.org/10.1002/ana.25651.
Von Ellenrieder, N., Gotman, J., Zelmann, R., et al., 2020. How the human brain sleeps: direct cortical recordings of normal brain activity. Ann. Neurol. 87 (2), 289–301. https://doi.org/10.1002/ana.25651.
Ward, LM., 2003. Synchronous neural oscillations and cognitive processes. Trends Cogn. Sci. 7 (12), 553–559. https://doi.org/10.1016/j.tics.2003.10.012.
Wei, X., Avigdor, T., Ho, A., et al., 2024. ANPHY-Sleep: an open sleep database from healthy adults using high-density scalp electroencephalogram. Sci. Data 11 (1), 896. https://doi.org/10.1038/s41597-024-03722-1.
Wiesman, A.I., da, Silva, Castanheira, J., Baillet, S., 2022. Stability of spectral estimates in resting-state magnetoencephalography: Recommendations for minimal data duration with neuroanatomical specificity. NeuroImage 247, 118823. https://doi.org/10.1016/j.neuroimage.2021.118823.
Zhou, S., Morgan, K., Hathaway, E., et al., 2023. High-Resolution EEG Characterization of Sleep Neurophysiology. In: Thomas, R.J., Bhat, S., Chokroverty, S. (Eds.), Atlas of Sleep Medicine. Springer International Publishing, Cham, pp. 389–415. https://doi.org/10.1007/978-3-031-34625-5_23.
Zorzos, I., Kakkos, I., Ventouras, E.M., Matsopoulos, GK., 2021. Advances in electrical source imaging: a review of the current approaches, applications and challenges. Signals 2 (3), 378–391. https://doi.org/10.3390/signals2030024.